RADAR CROSS SECTION (RCS)

RANDRIANANDRASANA Marie Emile [1], RANDRIAMITANTSOA Paul Auguste[2], RANDRIAMITANTSOA Andry Auguste[3]

[1]*Dept. of Telecommunication, Antsirabe Vankinankaratra High Education Institute,*

University of Antananarivo, Madagascar,

[2]*Dept. of Telecommunication, High School Polytechnic of Antananarivo,*

University of Antananarivo, Madagascar,

[3]*Dept. of Telecommunication, High School Polytechnic of Antananarivo,*

University of Antananarivo, Madagascar,

ABSTRACT

The research of Radar Cross Section or RCS of simple and complex objects is decisively important to identify targets. Knowing the statistical characteristics of a target's RCS is crucial to the success of radar target detection algorithms. The RCS of any reflector may be thought of **as** the projected area of equivalent isotropic reflector. The equivalent reflector returns the same power per unit solid angle**.** The term RCS was used to describe the amount of scattered power from a target towards the radar, when the target is illuminated by RF energy. At that time, RCS was referred to as a target-specific constant. This was only a simplification and, in practice, it is rarely the case. In this chapter, the phenomenon of target scattering and methods of RCS calculation are examined. Target RCS fluctuations due to aspect angle, frequency, and polarization are presented. Radar cross section characteristics of some simples and complex targets are also introduced and treated.

Keywords: Radar Cross Section, target, reflector, isotropic, scattered, illuminated, polarization

1. INTRODUCTION

When a target is illuminated by RF energy, it acts like an antenna, and will have near and far fields. Waves reflected and measured in the near field are, in general, spherical. Alternatively, in the far field the wave fronts are decomposed into a linear combination of plane waves. Assume the power density of a wave incident on a target located at range *R* away from the radar is P_{Di}. The amount of reflected power from the target is

$$\mathrm{P_r} = \sigma P_{Di} \tag{1}$$

σ denotes the target cross section. Define P_{Dr} as the power density of the scattered waves at the receiving antenna. It follows that

$$P_{Dr} = \frac{\mathrm{P_r}}{4\pi R^2} \tag{2}$$

remplacing P_r in (2) by its value in (1) we have

$$\sigma = 4\pi R^2 \left(\frac{P_{Dr}}{P_{Di}} \right) \tag{3}$$

and in order to ensure that the radar receiving antenna is in the far field (i.e., scattered waves received by the antenna are planar), we can modify (3) to

$$\sigma = 4\pi \lim_{R\to\infty} R^2 \left(\frac{P_{Dr}}{P_{Di}} \right) \tag{4}$$

The RCS defined by the equation (4) is often referred to as either the monostatic RCS, the backscattered RCS, or

simply target RCS. The backscattered RCS is measured from all waves scattered in the direction of the radar and has the same polarization as the receiving antenna. It represents a portion of the total scattered target RCS σ_t, where $\sigma_t > \sigma$. Assuming a spherical coordinate system defined by (ρ, θ, ϕ), then at range ρ the target scattered cross section is a function of (θ, ϕ). Let the angles (θ_i, ϕ_i) define the direction of propagation of the incident waves. Also, let the angles (θ_s, ϕ_s) define the direction of propagation of the scattered waves. The special case, When $\theta_s = \theta_i$ and $\phi_s = \phi_i$ defines the monostatic RCS. The RCS measured by the radar at angles $\theta_s \neq \theta_i$ and $\phi_s \neq \phi_i$ is called the bistatic RCS. The total target scattered RCS is given by

$$\sigma_t = \frac{1}{4\pi} \int_{\varphi_s=0}^{2\pi} \int_{\theta_s=0}^{2\pi} \sigma(\theta_s, \varphi_s) \sin\theta_s d\theta_s d\varphi_s \tag{5}$$

The amount of backscattered waves from a target is proportional to the ratio of the target extent (size) to the wavelength, λ, of the incident waves. In fact, a radar will not be able to detect targets much smaller than its operating wavelength. For example, if weather radars use L-band frequency, rain drops become nearly invisible to the radar since they are much smaller than the wavelength. RCS measurements in the frequency region, where the target extent and the wavelength are comparable, are referred to as the Rayleigh region. Alternatively, the frequency region where the target extent is much larger than the radar operating wavelength is referred to as the optical region.
In practice, the majority of radar applications fall within the optical region.
The analysis presented in this book mainly assumes far field monostatic RCS measurements in the optical region. Near field RCS, bistatic RCS, and RCS measurements in the Rayleigh region will not be considered since their treatment falls beyond this book.s intended scope. Additionally, RCS treatment in this chapter is mainly concerned with Narrow Band (NB) cases. In other words, the extent of the target under consideration falls within a single range bin of the radar. Wide Band (WB) RCS measurements will be briefly addressed in a later section. Wide band radar range bins are small (typically 10 - 50 cm); hence, the target under consideration may cover many range bins. The RCS value in an individual range bin corresponds to the portion of the target falling within that bin.

2. RCS PREDICTION METHODS

Most radar systems use RCS as a means of discrimination. Therefore, accurate prediction of target RCS is critical in order to design and develop robust discrimination algorithms. Additionally, measuring and identifying the scattering centers (sources) for a given target aid in developing RCS reduction techniques. Two categories of RCS prediction methods are available: exact and approximate. Exact methods of RCS prediction are very complex even for simple shape objects. This is because they require solving either differential or integral equations that describe the scattered waves from an object under the proper set of boundary conditions. Such boundary conditions are governed by Maxwell's equations. Even when exact solutions are achievable, they are often difficult to interpret and to program using digital computers. Due to the difficulties associated with the exact RCS prediction, approximate methods become the viable alternative. The majority of the approximate methods are valid in the optical region, and each has its own strengths and limitations. Most approximate methods can predict RCS within few dBs of the truth. Some of the most commonly used approximate methods are Geometrical Optics (GO), Physical Optics (PO), Geometrical Theory of Diffraction (GTD), Physical Theory of Diffraction (PTD), and Method of Equivalent Currents (MEC). Interested readers may consult Knott or Ruck (see bibliography) for more details on these and other approximate methods.

3. Dependency on Aspect Angle and Frequency

Radar cross section fluctuates as a function of radar aspect angle and frequency. For the purpose of illustration, isotropic point scatterers are considered. An isotropic scatterer is one that scatters incident waves equally in all directions.
For example, two unity ($1m^2$) isotropic scatterers are aligned and placed along the radar line of sight (zero aspect angle) at a far field range. The spacing between the two scatterers is 1 meter. The radar aspect angle is then changed from zero to 180 degrees, and the composite RCS of the two scatterers measured by the radar is computed.
This composite RCS consists of the superposition of the two individual radar cross sections. At zero aspect angle, the composite RCS is $2m^2$. Taking scatterer-1 as a phase reference, when the aspect angle is varied, the composite RCS is modified by the phase that corresponds to the electrical spacing between the two scatterers. For example, at aspect angle 10°, the electrical spacing between the two scatterers is

$$\text{elec-spacing} = \frac{2 \times (1.0 \times \cos(10°))}{\lambda} \tag{6}$$

with λ is the radar operating wavelength.

RCS is dependent on the radar aspect angle; thus, knowledge of this constructive and destructive interference between the individual scatterers can be very critical when a radar tries to extract the RCS of complex or maneuvering targets. This is true because of two reasons. First, the aspect angle may be continuously changing. Second, complex target RCS can be viewed to be made up from contributions of many individual scattering points distributed on the target surface. These scattering points are often called scattering centers. Many approximate RCS prediction methods generate a set of scattering centers that define the backscattering characteristics of such complex targets.

Next, to demonstrate RCS dependency on frequency, consider the following experiment : two far field unity isotropic scatterers are aligned with radar line of sight, and the composite RCS is measured by the radar as the frequency is varied from 8 GHz to 12.5 GHz (X-band). In this case, RCS fluctuation as a function of frequency is evident. Little frequency change can cause serious RCS fluctuation when the scatterer spacing is large. Alternatively, when scattering centers are relatively close, it requires more frequency variation to produce significant RCS fluctuation.

Assume that the two scatterers complete a full revolution about the radar line of sight in T_{rev} = 3 sec. Furthermore, assume that an X-band radar (f_0 = 9 GHz) is used to detect (observe) those two scatterers using a PRF f_r = 300 Hz for a period of 3 seconds. Finally, assume a *NB* bandwidth B_{NB} = *1 MHz* and a *WB* bandwidth . It follows that the radar.s *NB* and *WB* range resolutions are respectively equal to ΔR_{NB} = 150 m and ΔR_{WB} = 7.5 cm. Clearly, the two scatterers are completely contained within one range bin. The two scatterers are now completely resolved as two distinct scatterers, except during the times where both point scatterers fall within the same range bin.

4. RCS DEPENDENCY ON POLARIZATION

The material in this section covers two topics. First, a review of polarization fundamentals is presented. Second, the concept of the target scattering matrix is introduced.

The x and y electric field components for a wave traveling along the positive z direction are given by

$$E_x = E_1 \sin(\omega t - kz) \tag{7}$$

$$E_y = E_2 \sin(\omega t - kz + \delta) \tag{8}$$

where $k = 2\pi/\lambda$, ω is the wave frequency, the angle δ is the time phase angle which E_y leads E_x, and, finally, E_1 and E_2 are, respectively, the wave amplitudes along the x and y directions. When two or more electromagnetic waves combine, their electric fields are integrated vectorially at each point in space for any specified time. In general, the combined vector traces an ellipse when observed in the x-y plane.

The ratio of the major to the minor axes of the polarization ellipse is called the Axial Ratio (*AR*). When *AR* is unity, the polarization ellipse becomes a circle, and the resultant wave is then called circularly polarized. Alternatively, when E_1=0 and *AR*=∞ the wave becomes linearly polarized.

The equation (7) and (8) can be combined to give the instantaneous total electric field,

$$\vec{E} = \hat{a}_x E_1 \sin(\omega t - kz) + \hat{a}_y E_2 \sin(\omega t - kz + \delta) \tag{9}$$

where $\hat{a}_x$ and $\hat{a}_y$ are unit vectors along the *x* and *y* directions, respectively. At *z* = 0, $E_x = E_1 sin(\omega t)$ and $E_y = E_2 sin(\omega t + \delta)$, then by replacing by the ratio and by using trigonometry properties equation (9) can be rewritten as

$$\frac{E_x^{\,2}}{E_1^{\,2}} - \frac{2E_x E_y \cos\delta}{E_1 E_2} + \frac{E_y^{\,2}}{E_1^{\,2}} = (\sin\delta)^2 \tag{10}$$

Note that equation (10) has no dependency on ω_t.

In the most general case, the polarization ellipse may have any orientation. The angle is called the tilt angle of the ellipse. In this case, *AR* is given by

$$AR = \frac{OA}{OB}; (1 \le AR \le \infty) \tag{11}$$

When E_1 = 0, the wave is said to be linearly polarized in the y direction, while if E_2 = 0 the wave is said to be linearly polarized in the x direction. Polarization can also be linear at an angle of 45° when $E_1 = E_2$ and ξ = 45°. When $E_1 = E_2$ and δ = 90° the wave is said to be Left Circularly Polarized (LCP), while if δ = -90° the wave is said to Right Circularly Polarized (RCP). It is a common notation to call the linear polarizations along the x and y directions by the names horizontal and vertical polarizations, respectively.

In general, an arbitrarily polarized electric field may be written as the sum of two circularly polarized fields. More precisely,

$$\vec{E} = \overrightarrow{E_R} + \overrightarrow{E_L} \tag{12}$$

where $\overrightarrow{E_R}$ and $\overrightarrow{E_L}$ are the RCP and LCP fields, respectively. Similarly, the RCP and LCP waves can be written as

$$\overrightarrow{E_R} = \overrightarrow{E_V} + j\overrightarrow{E_H} \tag{13}$$

$$\overrightarrow{E_L} = \overrightarrow{E_V} - j\overrightarrow{E_H} \tag{14}$$

where $\overrightarrow{E_V}$ and $\overrightarrow{E_H}$ are the fields with vertical and horizontal polarizations, respectively. Combining the equations (13) and (14) yields

$$E_R = \frac{E_H - jE_V}{\sqrt{2}} \tag{15}$$

$$E_L = \frac{E_H + jE_V}{\sqrt{2}} \tag{16}$$

Using matrix notation the equations (15) and (16) can be rewritten as

$$\begin{bmatrix} E_R \\ E_L \end{bmatrix} = \frac{1}{\sqrt{2}} \begin{pmatrix} 1 & -j \\ 1 & j \end{pmatrix} \begin{bmatrix} E_H \\ E_V \end{bmatrix} = [T] \begin{bmatrix} E_H \\ E_V \end{bmatrix} \tag{17}$$

$$\begin{bmatrix} E_H \\ E_V \end{bmatrix} = \frac{1}{\sqrt{2}} \begin{pmatrix} 1 & 1 \\ j & -j \end{pmatrix} \begin{bmatrix} E_R \\ E_L \end{bmatrix} = [T]^{-1} \begin{bmatrix} E_R \\ E_L \end{bmatrix} \tag{18}$$

For many targets the scattered waves will have different polarization than the incident waves. This phenomenon is known as depolarization or cross-polarization. However, perfect reflectors reflect waves in such a fashion that an incident wave with horizontal polarization remains horizontal, and an incident wave with vertical polarization remains vertical but is phase shifted . Additionally, an incident wave which is RCP becomes LCP when reflected, and a wave which is LCP becomes RCP after reflection from a perfect reflector. Therefore, when a radar uses LCP waves for transmission, the receiving antenna needs to be RCP polarized in order to capture the PP RCS, and LCR to measure the OP RCS.

Target backscattered RCS is commonly described by a matrix known as the scattering matrix, and is denoted by *[S]*. When an arbitrarily linearly polarized wave is incident on a target, the backscattered field is then given by

$$\begin{bmatrix} E_1^s \\ E_2^s \end{bmatrix} = [S] \begin{bmatrix} E_1^i \\ E_2^i \end{bmatrix} = \begin{pmatrix} s_{11} & s_{12} \\ s_{21} & s_{22} \end{pmatrix} \begin{bmatrix} E_1^i \\ E_2^i \end{bmatrix} \tag{19}$$

The superscripts *i* and *s* denote incident and scattered fields. The quantities s_{ij} are in general complex and the subscripts *1* and *2* represent any combination of orthogonal polarizations. More precisely, *1 = H,R*, and *2 = V,L*. From the equation (1.03), the backscattered RCS is related to the scattering matrix components by the following relation :

$$\begin{pmatrix} \sigma_{11} & \sigma_{12} \\ \sigma_{21} & \sigma_{22} \end{pmatrix} = 4\pi R^2 \begin{pmatrix} |s_{11}|^2 & |s_{12}|^2 \\ |s_{21}|^2 & |s_{22}|^2 \end{pmatrix} \tag{20}$$

It follows that once a scattering matrix is specified, the target backscattered RCS can be computed for any combination of transmitting and receiving polarizations. The reader is advised to see Ruck for ways to calculate the scattering matrix *[S]*.

Rewriting the equation (20) in terms of the different possible orthogonal polarizations yields

$$\begin{bmatrix} E_H^s \\ E_V^s \end{bmatrix} = \begin{pmatrix} s_{HH} & s_{HV} \\ s_{VH} & s_{VV} \end{pmatrix} \begin{bmatrix} E_H^i \\ E_V^i \end{bmatrix} \tag{21}$$

$$\begin{bmatrix} E_R^s \\ E_L^s \end{bmatrix} = \begin{pmatrix} s_{RR} & s_{RL} \\ s_{LR} & s_{LL} \end{pmatrix} \begin{bmatrix} E_R^i \\ E_L^i \end{bmatrix} \tag{22}$$

By using the transformation matrix *[T]* in equation (17), the circular scattering elements can be computed from the linear scattering elements

$$\begin{pmatrix} s_{RR} & s_{RL} \\ s_{LR} & s_{LL} \end{pmatrix} = [T] \begin{pmatrix} s_{HH} & s_{HV} \\ s_{VH} & s_{VV} \end{pmatrix} \begin{pmatrix} 1 & 0 \\ 0 & -1 \end{pmatrix} [T]^{-1} \tag{23}$$

and the individual components are

$$\left\{ \begin{aligned} s_{RR} &= \frac{-s_{VV} + s_{HH} - j(s_{HV} + s_{VH})}{2} \\ s_{RL} &= \frac{s_{VV} + s_{HH} + j(s_{HV} - s_{VH})}{2} \\ s_{LR} &= \frac{s_{VV} + s_{HH} - j(s_{HV} - s_{VH})}{2} \\ s_{LL} &= \frac{-s_{VV} + s_{HH} + j(s_{HV} + s_{VH})}{2} \end{aligned} \right\} \tag{24}$$

Similarly, the linear scattering elements are given by

$$\begin{pmatrix} s_{HH} & s_{HV} \\ s_{VH} & s_{VV} \end{pmatrix} = [T]^{-1} \begin{pmatrix} s_{RR} & s_{RL} \\ s_{LR} & s_{LL} \end{pmatrix} \begin{pmatrix} 1 & 0 \\ 0 & -1 \end{pmatrix} [T] \tag{25}$$

and the individual components for that one are

$$\left\{ \begin{aligned} s_{HH} &= \frac{-s_{RR} + s_{RL} + s_{LR} - s_{LL}}{2} \\ s_{VH} &= \frac{j(s_{RR} + s_{RL} - s_{LR} - s_{LL})}{2} \\ s_{HV} &= \frac{-j(s_{RR} - s_{RL} + s_{LR} - s_{LL})}{2} \\ s_{VV} &= \frac{s_{RR} + s_{LL} + js_{RL} + s_{LR}}{2} \end{aligned} \right\} \tag{26}$$

5. RCS DEPENDENCY OF SIMPLE OBJECTS

In all cases, except for the perfectly conducting sphere, only optical region approximations are presented. Radar designers and RCS engineers consider the perfectly conducting sphere to be the simplest target to examine. Even in this case, the complexity of the exact solution, when compared to the optical region approximation, is overwhelming. Most formulas presented are Physical Optics (PO) approximation for the backscattered RCS measured by a far field radar in the direction (θ,ϕ),

In this section, it is assumed that the radar is always illuminating an object from the positive *z*-direction.

Due to symmetry, waves scattered from a perfectly conducting sphere are co-polarized (have the same polarization)

with the incident waves. This means that the cross-polarized backscattered waves are practically zero. For example, if the incident waves were Left Circularly Polarized (LCP), then the backscattered waves will also be LCP. However, because of the opposite direction of propagation of the backscattered waves, they are considered to be Right Circularly Polarized (RCP) by the receiving antenna. Therefore, the PP backscattered waves from a sphere are LCP, while the OP backscattered waves are negligible.

The normalized exact backscattered RCS for a perfectly conducting sphere is a Mie series given by

$$\frac{\sigma}{\pi r^2} = \left(\frac{j}{kr}\right)\sum_{n=1}^{\infty}(-1)^n(2n+1)\left(\frac{krJ_{n-1}(kr) - nJ_n(kr)}{krH_{n-1}^{(1)}(kr) - nH_n^{(1)}(kr)} - \frac{J_n(kr)}{H_n^{(1)}(kr)}\right) \tag{27}$$

where r is the radius of the sphere, $k = 2\pi/\lambda$, λ, is the wavelength, J_n is the spherical Bessel of the first kind of order n, and $H_n^{(1)}$ is the Hankel function of order n, and is given by

$$H_n^{(1)}(kr) = J_n(kr) + jY_n(kr) \tag{28}$$

Y_n is the spherical Bessel function of the second kind of order n.

We can specify three regions**:**

- the Optical region which corresponds to a large Sphere

$$\sigma = \pi r^2 \Leftrightarrow r \square \quad \lambda \tag{29}$$

- the Mie or Resonance region which is oscillatory in nature
- And the Rayleihg region corresponds to a small Sphere

$$\sigma \approx 9\pi r^2 (kr)^4 \Leftrightarrow r \square \quad \lambda \tag{30}$$

The backscattered RCS for a perfectly conducting sphere is constant in the optical region. For this reason, radar designers typically use spheres of known cross sections to experimentally calibrate radar systems. For this purpose, spheres are flown attached to balloons. In order to obtain Doppler shift, spheres of known RCS are dropped out of an airplane and towed behind the airplane whose velocity is known to the radar.

An ellipsoid centered at (0,0,0) is defined by the following equation :

$$\left(\frac{x}{a}\right)^2 + \left(\frac{y}{b}\right)^2 + \left(\frac{z}{c}\right)^2 = 1 \tag{31}$$

One widely accepted approximation for the ellipsoid backscattered RCS is given by

$$\sigma = \frac{\pi(a \times b \times c)^2}{\left[\left(a\sin(\theta)\cos(\varphi)\right)^2 + \left(b\sin(\theta)\sin(\varphi)\right)^2 + \left(c\cos(\theta)\right)^2\right]^2} \tag{32}$$

when $a = b$, the ellipsoid becomes roll symmetric and the RCS is independant of ϕ and the equation (5.06) is reduced to

$$\sigma = \frac{\pi b^4 c^2}{\left[\left(b\sin(\theta)\right)^2 + \left(c\cos(\theta)\right)^2\right]^2} \tag{33}$$

When $a = b = c$ so the equation (32) becomes

$$\sigma = \pi c^2 \tag{34}$$

and the equation (34) defines the backscattered RCS of a sphere. This should be expected, since under the condition $a = b = c$ the ellipsoid becomes a sphere. And due to the circular symmetry, the backscattered RCS of a circular flat plate has no dependency on ϕ. The RCS just depends only to the aspect angle. And for normal incidence, actually zero aspect angle ($\theta = 0°$), the backscattered RCS for a circular flat plate is

$$\sigma = \frac{4\pi^3 r^4}{\lambda^2} \tag{35}$$

For non-normal incidence ($\theta \neq 0°$), two approximations for the circular flat plate backscattered RCS for any linearly polarized incident wave are

$$\sigma = \frac{\lambda r}{8\pi \sin(\theta)(\tan(\theta))^2} \tag{36}$$

$$\sigma = \pi k^2 r^4 \left(\frac{2J_1(2kr\sin(\theta))}{2kr\sin(\theta)} \right)^2 (\cos(\theta))^2 \tag{37}$$

where $k = 2\pi/\lambda$, and $J_1(\beta)$ is the first order spherical Bessel function evaluated at β.
The half cone angle of frustum is given by

$$\tan(\alpha) = \frac{r_2 - r_1}{H} = \frac{r_2}{L} \tag{38}$$

Define the aspect angle at normal incidence with respect to the frustum's surface (broadside) as θ_n. Thus, when a frustum is illuminated by a radar located at the same side as the cone.s small end, the angle θ_n is

$$\theta_n = 90° - \alpha \tag{39}$$

Alternatively, normal incidence occurs at

$$\theta_n = 90° + \alpha \tag{40}$$

At normal incidence, one approximation for the backscattered RCS of a truncated cone due to a linearly polarized incident wave is

$$\sigma_{\theta_n} = \frac{8\pi \left(z_2^{3/2} - z_2^{3/2} \right)^2}{9\lambda \sin(\theta_n)} \tan(\alpha)[\sin(\theta_n) - \cos(\theta_n)\tan(\alpha)]^2 \tag{41}$$

where λ is the wavelength. Using trigonometric identities, the equation (41) can be reduced to

$$\sigma_{\theta_n} = \frac{8\pi \left(z_2^{3/2} - z_2^{3/2} \right)^2}{9\lambda} \frac{\sin(\alpha)}{(\cos(\alpha))^4} \tag{42}$$

For non-normal incidence, the backscattered RCS due to a linearly polarized incident wave is

$$\sigma = \frac{\lambda z \tan(\alpha)}{8\pi \sin(\theta)} \left(\frac{\sin(\theta) - \cos(\theta)\tan(\alpha)}{\sin(\theta)\tan(\alpha) + \cos(\theta)} \right)^2 \tag{43}$$

where z is equal to either z_1 or z_2 depending on whether the RCS contribution is from the small or the large end of the cone. Again, using trigonometric identities, supposed that the radar illuminates the starting from the large end, the equation (43) is reduced to

$$\sigma = \frac{\lambda z \tan(\alpha)}{8\pi \sin(\theta)} (\tan(\theta - \alpha))^2 \tag{44}$$

When the radar illuminates the frustum starting from the small end, namely the radar is in the negative z direction**,** so the equation (44) should be modified to

$$\sigma = \frac{\lambda z \tan(\alpha)}{8\pi \sin(\theta)} (\tan(\theta + \alpha))^2 \tag{45}$$

Two cases are presented: first, the general case of an elliptical cross section cylinder; second, the case of a circular cross section cylinder. The normal and non-normal incidence backscattered RCS due to a linearly polarized incident wave from an elliptical cylinder with minor and major radii being r_1 and r_2 are, respectively, given by

$$\sigma_{\theta_n} = \frac{2\pi\left(H \times r_1 \times r_2\right)^2}{\lambda\left[\left(r_1\cos(\varphi)\right)^2 + \left(r_2\,\mathrm{s}\,in(\varphi)\right)^2\right]^{3/2}} \tag{46}$$

$$\sigma = \frac{\lambda\left(r_1 \times r_2\right)^2 \sin(\theta)}{8\pi(\cos(\theta))^2\left[\left(r_1\cos(\varphi)\right)^2 + \left(r_2\,\mathrm{s}\,in(\varphi)\right)^2\right]^{3/2}} \tag{47}$$

For a circular cylinder of radius *r*, then due to roll symmetry, the equations (46) and (47), respectively, reduce to

$$\sigma_{\theta_n} = \frac{2\pi H^2 r}{\lambda} \tag{48}$$

$$\sigma = \frac{\lambda r \sin(\theta)}{8\pi(\cos(\theta))^2} \tag{49}$$

Consider a perfectly conducting rectangular thin flat plate in the *x-y* plane. The two sides of the plate are denoted by *2a* and *2b*. For a linearly polarized incident wave in the *x-z* plane, the horizontal and vertical backscattered RCS are, respectively, given by4

$$\sigma_V = \frac{b^2}{\pi}\left|\sigma_{1V} - \sigma_{2V}\left[\frac{1}{\cos(\theta)} + \frac{\sigma_{2V}}{4}(\sigma_{3V} + \sigma_{4V})\right]\sigma_{5V}^{-1}\right|^2 \tag{50}$$

$$\sigma_H = \frac{b^2}{\pi}\left|\sigma_{1H} - \sigma_{2H}\left[\frac{1}{\cos(\theta)} - \frac{\sigma_{2H}}{4}(\sigma_{3H} + \sigma_{4H})\right]\sigma_{5H}^{-1}\right|^2 \tag{51}$$

where $k = 2\pi/\lambda$ and

$$\sigma_{1V} = \sigma_{1H} = \cos(ka\sin(\theta)) - j\frac{\sin(ka\sin(\theta))}{\sin(\theta)} \tag{52}$$

$$\sigma_{2V} = \frac{e^{j\left(ka - \frac{\pi}{4}\right)}}{\sqrt{2\pi}(ka)^{\frac{3}{2}}} \tag{53}$$

$$\sigma_{3V} = \frac{(1+\sin(\theta))e^{-jka\sin(\theta)}}{(1-\sin(\theta))^2} \tag{54}$$

$$\sigma_{4V} = \frac{(1-\sin(\theta))e^{jka\sin(\theta)}}{(1+\sin(\theta))^2} \tag{55}$$

$$\sigma_{5V} = 1 - \frac{e^{j\left(2ka - \frac{\pi}{2}\right)}}{8\pi(ka)^3} \tag{56}$$

$$\sigma_{2H} = \frac{4e^{j(ka+\frac{\pi}{4})}}{\sqrt{2\pi}(ka)^{\frac{1}{2}}} \tag{57}$$

$$\sigma_{3H} = \frac{e^{-jka\sin(\theta)}}{1-\sin(\theta)} \tag{58}$$

$$\sigma_{4H} = \frac{e^{jka\sin(\theta)}}{1+\sin(\theta)} \tag{59}$$

$$\sigma_{5H} = 1-\frac{e^{j(2ka+\frac{\pi}{2})}}{2\pi(ka)} \tag{60}$$

The equations (50) and (51) are valid and quite accurate for aspect angles 0°≤θ≤80. For aspect angles near 90°, Ross obtained by extensive fitting of measured data an empirical expression for the RCS. It is given by

$$\sigma_H \to 0$$

$$\sigma_V = \frac{ab^2}{\lambda}\left\{\left[1+\frac{\pi}{2(2a/\lambda)^2}\right]+\left[1-\frac{\pi}{2(2a/\lambda)^2}\right]\cos\left(2ka-\frac{3\pi}{5}\right)\right\} \tag{61}$$

The backscattered RCS for a perfectly conducting thin rectangular plate for incident waves at any θ, ϕ can be approximated by

$$\sigma = \frac{4\pi a^2 b^2}{\lambda^2}\left(\frac{\sin(ak\sin(\theta)\cos(\varphi))}{ak\sin(\theta)\cos(\varphi)}\frac{\sin(bk\sin(\theta)\cos(\varphi))}{bk\sin(\theta)\cos(\varphi)}\right)^2(\cos(\theta))^2 \tag{62}$$

The equation (62) is independent of the polarization, and is only valid for aspect angles θ≤20°.

Consider the triangular flat plate defined by the isosceles triangle. The backscattered RCS can be approximated for small aspect angles (θ≤30°) by

$$\sigma = \frac{4\pi A^2}{\lambda^2}(\cos(\theta))^2\sigma_0 \tag{63}$$

$$\sigma_0 = \frac{\left[\left(\sin(\alpha)\right)^2-(\sin(\beta/2))^2\right]^2+\sigma_{01}}{\alpha^2-(\beta/2)^2} \tag{64}$$

$$\sigma_{01} = \frac{1}{4}(\sin(\varphi))^2\left[\left(2a/b\right)\cos(\varphi)\sin(\beta)-\sin(\varphi)\,s\,in(2\alpha)\right]^2 \tag{65}$$

where $\alpha = k\,asin\theta cos(\phi)$, $\beta = kbsin\theta sin(\phi)$, and $A = ab/2$. For waves incident in the plane $\phi = 0$, the RCS reduced to

$$\sigma = \frac{4\pi A^2}{\lambda^2}(\cos(\theta))^2\left[\frac{(\sin(\alpha))^4}{\alpha^4} + \frac{(\sin(2\alpha)-2\alpha)^2}{4\alpha^4}\right] \tag{66}$$

and for the incidence $\phi = \pi/2$

$$\sigma = \frac{4\pi A^2}{\lambda^2}(\cos(\theta))^2\left[\frac{(\sin(\beta/2))^4}{(\beta/2)^4}\right] \tag{67}$$

6. SCATTERING FROM A DIELECTRIC-CAPPED WEDGE

The geometry of a dielectric-capped wedge is required to find to the field expressions for the problem of scattering by a 2-D perfect electric conducting (PEC) wedge capped with a dielectric cylinder. Using the cylindrical coordinates system, the excitation due to an electric line current of complex amplitude I_0 located at (ρ_0, ϕ_0) results in TM^z incident field with the electric field expression given by

$$E_z^i = -I_e \frac{\omega\mu_0}{4} H_0^{(2)}\left(k\left|\rho-\rho_0\right|\right) \tag{68}$$

The problem is divided into three regions, I, II, and III. The field expressions may be assumed to take the following forms :

$$\left\{\begin{aligned} E_z^I &= \sum_{n=0}^{\infty} a_n J_\nu\left(k_1\rho\right)\sin(\nu(\varphi-\alpha))\sin(\nu(\varphi_0-\alpha)) \\ E_z^{II} &= \sum_{n=0}^{\infty}\left(b_n J_\nu\left(k\rho\right)+c_n H_\nu^{(2)}\left(k\rho\right)\right)\sin(\nu(\varphi-\alpha))\sin(\nu(\varphi_0-\alpha)) \\ E_z^{III} &= \sum_{n=0}^{\infty} d_n H_\nu^{(2)}\left(k\rho\right)\sin(\nu(\varphi-\alpha))\sin(\nu(\varphi_0-\alpha)) \end{aligned}\right\} \tag{69}$$

Where

$$\nu = \frac{n\pi}{2\pi-\alpha-\beta} \tag{70}$$

while $J_\nu(x)$ is the Bessel function of order ν and argument x and $H_\nu^{(2)}$ is the Hankel function of the second kind of order ν and argument x. From Maxwell's equations, the magnetic field component H_ϕ is related to the electric field component E_z for a TM^z wave by

$$H_\varphi = \frac{1}{j\omega\mu}\frac{\partial E_z}{\partial\rho} \tag{71}$$

Thus, the magnetic field component H_ϕ in the various regions may be written as

$$\left\{\begin{aligned} E_\varphi^I &= \frac{k_1}{j\omega\mu_0}\sum_{n=0}^{\infty} a_n J_\nu'\left(k_1\rho\right)\sin(\nu(\varphi-\alpha))\sin(\nu(\varphi_0-\alpha)) \\ E_\varphi^{II} &= \frac{k}{j\omega\mu_0}\sum_{n=0}^{\infty}\left(b_n J_\nu'\left(k\rho\right)+c_n H_\nu^{(2)}{}'\left(k\rho\right)\right)\sin(\nu(\varphi-\alpha))\sin(\nu(\varphi_0-\alpha)) \\ E_\varphi^{III} &= \frac{k}{j\omega\mu_0}\sum_{n=0}^{\infty} d_n H_\nu^{(2)}{}'\left(k\rho\right)\sin(\nu(\varphi-\alpha))\sin(\nu(\varphi_0-\alpha)) \end{aligned}\right\} \tag{72}$$

Where the prime indicated derivatives with respect to the full argument of the function. The boundary conditions require that the tangential electric field components vanish at the PEC surface. Also, the tangential field components should be continuous across the air-dielectric interface and the virtual boundary between region II and III, except for the discontinuity of the magnetic field at the source point. Thus,

- at $\varphi = \alpha;\ 2\pi - \beta$

$$E_z = 0 \tag{73}$$

- at $\rho = a$

$$\left.\begin{aligned} E_z^I &= E_z^{II} \\ H_\varphi^I &= H_\varphi^{II} \end{aligned}\right\} \tag{74}$$

- at $\rho = \rho_0$

$$\left.\begin{aligned} E_z^I &= E_z^{III} \\ H_\varphi^{II} - H_\varphi^{III} &= -J_e \end{aligned}\right\} \tag{75}$$

The current density J_e may be given in Fourier series expansion as

$$J_e = \frac{I_e}{\rho_0}\delta(\varphi-\varphi_0) = \frac{2}{2\pi-\alpha-\beta}\frac{I_e}{\rho_0}\sum_{n=0}^{\infty}\sin(\nu(\rho-\alpha))\sin(\nu(\rho_0-\alpha)) \tag{76}$$

The boundary condition on the PEC surface is automatically satisfied by the dependence φ of the electric field equation (72). From the boundary conditions in equation (73)

$$\sum_{n=0}^{\infty} a_n J_\nu(k_1 a)\sin(\nu(\rho-\alpha))\sin(\nu(\rho_0-\alpha)) = \sum_{n=0}^{\infty}\left(b_n J_\nu(ka) + c_n H_\nu^{(2)}(ka)\right)\sin(\nu(\rho-\alpha))\sin(\nu(\rho_0-\alpha)) \tag{77}$$

$$\frac{k_1}{j\omega\mu_0}\sum_{n=0}^{\infty} a_n J_\nu'(k_1 a)\sin(\nu(\rho-\alpha))\sin(\nu(\rho_0-\alpha)) =$$

$$\frac{k}{j\omega\mu_0}\sum_{n=0}^{\infty}\left(b_n J_\nu'(ka) + c_n H_\nu^{(2)}'(ka)\right)\sin(\nu(\rho-\alpha))\sin(\nu(\rho_0-\alpha)) \tag{78}$$

From the boundary conditions in the equation (74), we have

$$\sum_{n=0}^{\infty}\left(b_n J_\nu(ka) + c_n H_\nu^{(2)}(ka)\right)\sin(\nu(\rho-\alpha))\sin(\nu(\rho_0-\alpha)) = \sum_{n=0}^{\infty} d_n H_\nu^{(2)}(k\rho)\sin(\nu(\varphi-\alpha))\sin(\nu(\varphi_0-\alpha)) \tag{79}$$

$$\frac{k}{j\omega\mu_0}\sum_{n=0}^{\infty}\left(b_n J_\nu'(k\rho) + c_n H_\nu^{(2)}'(k\rho)\right)\sin(\nu(\varphi-\alpha))\sin(\nu(\varphi_0-\alpha)) = \frac{k}{j\omega\mu_0}\sum_{n=0}^{\infty} d_n H_\nu^{(2)}'(k\rho)\sin(\nu(\varphi-\alpha))\sin(\nu(\varphi_0-\alpha))$$

$$-\frac{2}{2\pi-\alpha-\beta}\frac{I_e}{\rho_0}\sum_{n=0}^{\infty}\sin(\nu(\rho-\alpha))\sin(\nu(\rho_0-\alpha)) \tag{80}$$

Since the equation (77) and (80) hold for all , the series on the left and right hand sides should be equal term by term. More precisely,

$$a_n J_\nu(k_1 a) = b_n J_\nu(ka) + c_n H_\nu^{(2)}(ka) \tag{81}$$

$$\frac{k_1}{\mu_0} a_n J_v'(k_1 a) = \frac{k}{\mu_0}(b_n J_v'(ka) + c_n H_v^{(2)}{}'(ka)) \tag{82}$$

$$b_n J_v(k\rho_0) + c_n H_v^{(2)}(k\rho_0) = d_n H_v^{(2)}(k\rho_0) \tag{83}$$

$$b_n J_v'(k\rho_0) + c_n H_v^{(2)}{}'(k\rho_0) = d_n H_v^{(2)}(k\rho_0) - \frac{2j\eta_0}{2\pi-\alpha-\beta}\frac{I_e}{\rho_0} \tag{84}$$

From the equation (81) and (82), we have

$$a_n = \frac{1}{J_v(k_1 a)}\left[b_n J_v(ka) + c_n H_v^{(2)}(ka)\right] \tag{85}$$

$$d_n = c_n + b_n \frac{J_v(k\rho_0)}{H_v^{(2)}(k\rho_0)} \tag{86}$$

Multiplying the equation (83) by $H_v^{(2)\prime}$ and the equation (84) by $H_v^{(2)}$, and by subtraction and using the Wronskian of the Bessel and Hankel functions, we get

$$b_n = -\frac{\pi\omega\mu_0 I_e}{2\pi-\alpha-\beta} H_v^{(2)}(k\rho_0) \tag{87}$$

Substituting b_n in the equation (81) and (82) and solving for c_n yield

$$c_n = \frac{\pi\omega\mu_0 I_e}{2\pi-\alpha-\beta}\left[H_v^{(2)}(k\rho_0)\frac{kJ_v'(ka)J_v(k_1a) - k_1 J_v(ka)J_v'(k_1a)}{kH_v^{(2)}{}'(ka)J_v(k_1a) - k_1 H_v^{(2)}(ka)J_v'(k_1a)}\right] \tag{88}$$

From the equation (86) through (88), may be given by

$$d_n = \frac{\pi\omega\mu_0 I_e}{2\pi-\alpha-\beta}\left[H_v^{(2)}(k\vartheta_0)\frac{kJ_v'(ka)J_v(k_1a) - k_1 J_v(ka)J_v'(k_1a)}{kH_v^{(2)}{}'(ka)J_v(k_1a) - k_1 H_v^{(2)}(ka)J_v'(k_1a)} - J_v(k\rho_0)\right] \tag{89}$$

which can be written as

$$d_n = \frac{\pi\omega\mu_0 I_e}{2\pi-\alpha-\beta}\left\{\begin{array}{l} kJ_v(k_1a)\left[J_v'(ka)H_v^{(2)}(k\rho_0) - H_v^{(2)}{}'(ka)J_v(k\rho_0)\right] + K \\ \dfrac{kJ_v'(k_1a)\left[H_v^{(2)}(ka)J_v(k\rho_0) - J_v(ka)H_v^{(2)}(k\rho_0)\right]}{kH_v^{(2)}{}'(ka)J_v(k_1a) - k_1 H_v^{(2)}(ka)J_v'(k_1a)} \end{array}\right\} \tag{90}$$

Substituting for the Hankel function in terms of Bessel and Neumann functions, Ethe equation (90) reduces to

$$d_n = -j\frac{\pi\omega\mu_0 I_e}{2\pi-\alpha-\beta}\left\{\begin{array}{l} kJ_v(k_1a)\left[J_v'(ka)Y_v(k\rho_0) - Y_v'(ka)J_v(k\rho_0)\right] + K \\ \dfrac{kJ_v'(k_1a)\left[Y_v(ka)J_v(k\rho_0) - J_v(ka)Y_v(k\rho_0)\right]}{kH_v^{(2)}{}'(ka)J_v(k_1a) - k_1 H_v^{(2)}(ka)J_v'(k_1a)} \end{array}\right\} \tag{91}$$

With these closed form expressions for the expansion coeffiecients a_n, b_n, and c_n, d_n the field components E_z and H_ϕ can be determined from the equation (69) and the equation (72), respectively. Alternatively, the magnetic field component H_ρ can be computed from

$$H_\rho = -\frac{1}{j\omega\mu}\frac{1}{\rho}\frac{\partial E_z}{\partial \varphi} \tag{92}$$

Thus, the H_ρ expressions for the three regions are defined become

$$\left\{\begin{array}{l} H_\rho^I = -\dfrac{1}{j\omega\mu\rho}\displaystyle\sum_{n=0}^{\infty} a_n \nu J_\nu\left(k_1\rho\right)\cos(\nu(\varphi-\alpha))\sin(\nu(\varphi_0-\alpha)) \\ H_\rho^{II} = -\dfrac{1}{j\omega\mu\rho}\displaystyle\sum_{n=0}^{\infty} \nu\left(b_n J_\nu\left(k\rho\right)+c_n H_\nu^{(2)}{}'\left(k\rho\right)\right)\cos(\nu(\varphi-\alpha))\sin(\nu(\varphi_0-\alpha)) \\ H_\rho^{III} = -\dfrac{1}{j\omega\mu\rho}\displaystyle\sum_{n=0}^{\infty} d_n \nu H_\nu^{(2)}\left(k\rho\right)\cos(\nu(\varphi-\alpha))\sin(\nu(\varphi_0-\alpha)) \end{array}\right\} \tag{93}$$

In region III, the scattered field may be found as the difference between the total and incident fields. Thus, using Eqs. (68) and (69) and considering the far field condition ($\rho \to \infty$) we get

$$\left\{\begin{array}{l} E_z^{III} = E_z^i + E_z^s = \sqrt{\dfrac{2j}{\pi k\rho}}e^{-jk\rho}\displaystyle\sum_{n=0}^{\infty} d_n j^\nu \sin(\nu(\varphi-\alpha))\sin(\nu(\varphi_0-\alpha)) \\ E_z^i = -I_e\dfrac{\omega\mu_0}{4}\sqrt{\dfrac{2j}{\pi k\rho}}e^{H_\rho} = -\dfrac{1}{j\omega\mu}\dfrac{1}{\rho}\dfrac{\partial E_z}{\partial\varphi} \end{array}\right\} \tag{94}$$

Note that d_n can be written as

$$d_n = -\frac{\omega\mu_0 I_e}{4} d_n^{\%} \tag{95}$$

where

$$d_n^{\%} = j\frac{4\pi}{2\pi-\alpha-\beta}\left\{\begin{array}{l} kJ_\nu(k_1a)\left[J_\nu{}'(ka)Y_\nu(k\rho_0)-Y_\nu{}'(ka)J_\nu(k\rho_0)\right]+K \\ \dfrac{kJ_\nu{}'(k_1a)\left[Y_\nu(ka)J_\nu(k\rho_0)-J_\nu(ka)Y_\nu(k\rho_0)\right]}{kH_\nu^{(2)}{}'(ka)J_\nu(k_1a)-k_1H_\nu^{(2)}(ka)J_\nu{}'(k_1a)} \end{array}\right\} \tag{96}$$

Substituting the equation (94) into the equation (93), the scattered field *f(ϕ)* is

$$E_z^s = -\frac{\omega\mu_0 I_e}{4}\sqrt{\frac{2j}{\pi k\rho}}e^{-jk\rho}\left(\sum_{n=0}^{\infty} d_n j^\nu \sin(\nu(\varphi-\alpha))\sin(\nu(\varphi_0-\alpha)) - e^{jk\rho_0\cos(\varphi-\varphi_0)}\right) \tag{97}$$

For plane wave excitation ($\rho_0 \to \infty$), the expression in the equations (87) and (88) reduce to

$$\left\{\begin{array}{l} b_n = -\dfrac{\pi\omega\mu_0 I_e}{2\pi-\alpha-\beta}\, j^\nu\sqrt{\dfrac{2j}{\pi k\rho_0}}e^{-jk\rho_0} \\ c_n = \dfrac{\pi\omega\mu_0 I_e}{2\pi-\alpha-\beta}\, j^\nu\sqrt{\dfrac{2j}{\pi k\rho_0}}e^{-jk\rho_0}\,\dfrac{kJ_\nu{}'(ka)J_\nu(k_1a)-k_1J_\nu(ka)J_\nu{}'(k_1a)}{kH_\nu^{(2)}{}'(ka)J_\nu(k_1a)-k_1H_\nu^{(2)}(ka)J_\nu{}'(k_1a)} \end{array}\right\} \tag{98}$$

where the complex amplitude of the incident plane wave, E_0, can be given by

$$E_0 = -I_e \frac{\omega\mu_0}{4}\sqrt{\frac{2j}{\pi k\rho_0}}e^{-jk\rho_0} \tag{99}$$

In this case, the field components can be evaluated in regions I and II only.
If $\alpha = \beta$ (reference at bisector); The definition of v reduces to

$$v = \frac{n\pi}{2(\pi-\beta)} \tag{100}$$

and the same expression will hold for the coefficients (with $\alpha = \beta$)
If $\alpha = 0$ (reference at face); the definition of v takes on the form

$$v = \frac{n\pi}{2\pi-\beta} \tag{101}$$

and the same expression will hold for the coefficients (with $\alpha = 0$)
If $k_1 \to \infty$ (PEC cap); Fields at region I will vanish, and the coefficients will be given by

$$\left\{\begin{aligned} b_n &= -\frac{\pi\omega\mu_0 I_e}{2\pi-\alpha-\beta}H_v^{(2)}(k\rho_0) \\ c_n &= \frac{\pi\omega\mu_0 I_e}{2\pi-\alpha-\beta}H_v^{(2)}(k\rho_0)\frac{J_v(ka)}{H_v^{(2)}(ka)} \\ d_n &= j\frac{\pi\omega\mu_0 I_e}{2\pi-\alpha-\beta}\frac{Y_v(ka)J_v(k\rho_0)-J_v(ka)Y_v(k\rho_0)}{H_v^{(2)}(ka)} \\ a_n &= \frac{1}{J_v(k_1a)}\left[b_nJ_v(ka)+c_nH_v^{(2)}(ka)\right]=0 \end{aligned}\right\} \tag{102}$$

Note that the expressions of b_n and a_n will yield zero tangential electric field at $\rho = a$ when substituted in the equation (69).
If $a \to 0$ (no cap); the expressions of the coefficients in this case may be obtained by setting $k_1 = k$, or by taking the limit as a approaches zero. Thus,

$$\left\{\begin{array}{l} c_n = \dfrac{\pi\omega\mu_0 I_e}{2\pi-\alpha-\beta}\left[H_\nu^{(2)}(k\rho_0)\dfrac{kJ_\nu'(ka)J_\nu(ka)-kJ_\nu(ka)J_\nu'(ka)}{kH_\nu^{(2)'}(ka)J_\nu(ka)-kH_\nu^{(2)}(ka)J_\nu'(ka)}\right]=0 \\ b_n = \dfrac{\pi\omega\mu_0 I_e}{2\pi-\alpha-\beta}H_\nu^{(2)}(k\rho_0)\dfrac{J_\nu(ka)}{H_\nu^{(2)}(ka)} \\ a_n = \dfrac{1}{J_\nu(ka)}\left[b_n J_\nu(ka)+c_n H_\nu^{(2)}(ka)\right]=b_n \\ d_n = \dfrac{\pi\omega\mu_0 I_e}{2\pi-\alpha-\beta}\left\{\dfrac{kJ_\nu(k_1a)\left[J_\nu'(ka)H_\nu^{(2)}(k\rho_0)-H_\nu^{(2)}'(ka)J_\nu(k\rho_0)\right]+K}{kH_\nu^{(2)'}(ka)J_\nu(k_1a)-k_1H_\nu^{(2)}(ka)J_\nu'(k_1a)}\right\}= \\ \quad = -\dfrac{\pi\omega\mu_0 I_e}{2\pi-\alpha-\beta}J_\nu(k\rho_0) \end{array}\right. \quad (103)$$

If $a \to 0$ and $\alpha = \beta = 0$ (semi-infinite PEC plane); In this case, the coefficients in the equation (6.36) become valid with the exception that the values of ν reduce to $n/2$. Once, the electric field component E_z in the different regions is computed, the corresponding magnetic field component H_ϕ can be computed using the equation (6.04) and the magnetic field component H_ρ may be computed as

$$H_\rho = -\frac{1}{j\omega\mu}\frac{1}{\rho}\frac{\partial E_z}{\partial\varphi} \quad (104)$$

7. *Triangular Flat Plate*

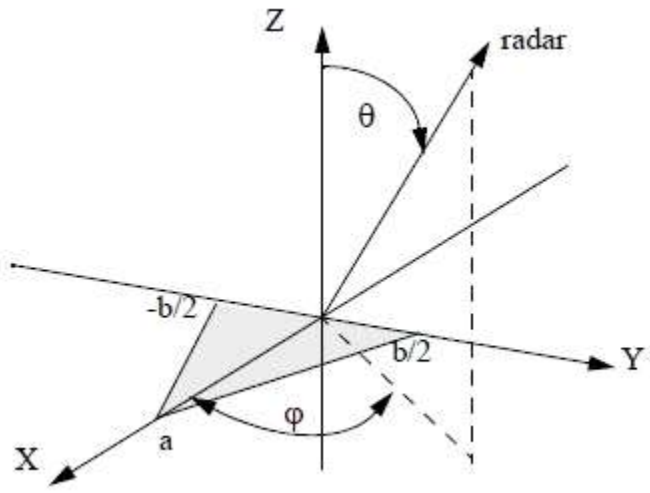

Fig1 : Coordinates for a perfectly conducting isosceles trinagular plate

Consider the triangular flat plate defined by the isosceles triangle as oriented in **Figure 1**.
Fig2 shows a plot for the normalized backscattered RCS from a perfectly conducting isosceles triangular flat plate.

The MATLAB function noted as *"rcs_isosceles.m"* which calculates and plots the backscattered RCS of a triangular flat plate.

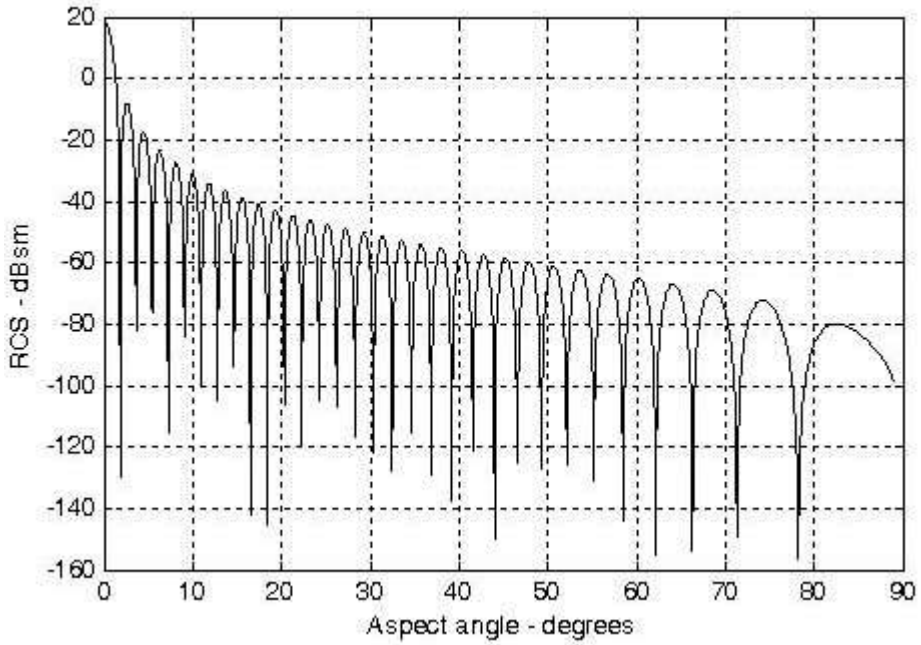

Fig2 : Backscattered RCS for a perfectly conducting triangular flat plate, with *a* = 20*cm* and *b* = 75*cm*

CONCLUSON

He study of radar sections takes a very large place today in the term of target detection and the improvement of radar applications. Radar researchers and designers, especially in powerful countries, never cease to improve their weapons through in-depth studies of RCS in the face of this threat of world war.

8. REFERENCES

[1] Jose M. Tamayo, Palau, Pascal De Resseguier "Simulation of Near Field RCS to Reproduce Measurement Condition"

[2] Woobin Kim, Hyeong-Rae Im, Yeong-Hoon Noh, Ic-Pyo Hong, Hyun-Sung Tae, Jeong-Kyu Kim, Jong-Gwan Yook "Near-Field to Far-Field RCS Prediction on Arbitrary Scanning Surfaces Based on Spherical Wave Expansion"

[3] Pofessor A. Manikas "Priciples of Classical and Modern Radar Radar Cross Section (RCS) and Radar Clutter (RC)"

[4] J. A. McEntee "A Technique For Measuring The Scattering Aperture And Absorption Aperture Of An Antenna"

[5] Levent Sevgi "RCS Measurements"

[6] Nicolas Asada "A Study of the Effect on Radar Cross Section (RCS) Due To 'Starved Horse Patterns' "

[7] Marcelo A. S. Miacci, Mirabel C. Rezende "Basics on Radar Cross Section Reduction Measurements of Simple and Complex Targets Using Microwave Absorbers"

[8]Juan M. Rius, Miguel Ferrando, Luis Jofre "High-Frequncy Radar Cross Section (RCS) of Complex Radar Targets in Real-Time"